J|A|C|S ARTICLES

Published on Web 06/03/2010

The Polar Phase of $NaNbO_3$: A Combined Study by Powder Diffraction, Solid-State NMR, and First-Principles Calculations

Karen E. Johnston,[†] Chiu C. Tang,[‡] Julia E. Parker,[‡] Kevin S. Knight,[§] Philip Lightfoot,*[,†] and Sharon E. Ashbrook*[,†]

School of Chemistry and EaStCHEM, University of St. Andrews, St. Andrews, KY16 9ST, U.K., Diamond Light Source Ltd., Harwell Science and Innovation Campus, Didcot, Oxfordshire, OX11 0DE, U.K., and ISIS Facility, Rutherford Appleton Laboratory, Chilton, Didcot, OX11 0QX, U.K.

Received March 5, 2010; E-mail: pl@st-and.ac.uk; sema@st-and.ac.uk

Abstract: A polar phase of $NaNbO_3$ has been successfully synthesized using sol-gel techniques. Detailed characterization of this phase has been undertaken using high-resolution powder diffraction (X-ray and neutron) and ^{23}Na multiple-quantum (MQ) MAS NMR, supported by second harmonic generation measurements and density functional theory calculations. Samples of $NaNbO_3$ were also synthesized using conventional solid-state methods and were observed to routinely comprise of a mixture of two different polymorphs of $NaNbO_3$, namely, the well-known orthorhombic phase (space group *Pbcm*) and the current polar phase, the relative quantities of which vary considerably depending upon precise reaction conditions. Our studies show that each of these two polymorphs of $NaNbO_3$ contains two crystallographically distinct Na sites. This is consistent with assignment of the polar phase to the orthorhombic space group $P2_1ma$, although peak broadenings in the diffraction data suggest a subtle monoclinic distortion. Using carefully monitored molten salt techniques, it was possible to eradicate the polar polymorph and synthesize the pure *Pbcm* phase.

Introduction

Sodium niobate, $NaNbO_3$, is a perovskite that is of significant interest at present owing to recent reports of exceptional piezoelectric responses in $NaNbO_3$-derived ceramics such as the solid-solution $K_xNa_{1-x}NbO_3$ (KNN); these properties have the potential to make KNN-based ceramics a viable lead-free alternative to the most widely used piezoelectric material $Pb(Zr_xTi_{1-x})O_3$ (PZT).[1,2] In recent years research on the KNN system has accelerated, with studies concentrated, in particular, around the $x = 0.5$ region of the phase diagram at the suggested morphotropic phase boundary (MPB), where the highest piezoelectric responses were initially located. Ultimately, however, to fully understand this system, each end-member in the solid-solution requires complete structural characterization. While the crystal structure of the room temperature form of $KNbO_3$ is widely accepted as orthorhombic, in space group $Amm2$,[3] with $a = 3.971$ Å, $b = 5.697$ Å and $c = 5.723$ Å, the various polymorphs of $NaNbO_3$ are still a subject of significant discussion. $NaNbO_3$ possesses an extremely complex phase diagram containing a series of complicated and poorly understood phase transitions as a function of temperature.[4−8] In more recent work, the existence of several new room temperature polymorphs of $NaNbO_3$ has been suggested.[9,10] In light of these recent findings, in addition to the existing ambiguities regarding the various $NaNbO_3$ polymorphs,[5] the present work concentrates on the synthetic chemistry and structural characterization of the room temperature polymorphs of $NaNbO_3$.

Published crystallographic data indicate that the most commonly reported room temperature phase of $NaNbO_3$ has an orthorhombic unit cell, space group *Pbcm*, with $a = 5.506$ Å, $b = 5.566$ Å, and $c = 15.520$ Å (Figure 1a). This phase, first characterized by Sakowski-Cowley et al.,[7] displays an unusual "octahedral tilting" scheme with three independent tilts leading to a $\sqrt{2}a_p \times \sqrt{2}a_p \times 4a_p$ supercell of the basic cubic perovskite subcell, where a_p is the idealized cubic perovskite lattice parameter, ~3.9 Å.[11] This structure possesses two crystallographically distinct Na sites. However, on the basis of peak broadenings observed using high-resolution neutron powder diffraction, Darlington and Knight suggest this phase is actually monoclinic, with $\gamma = 89.94°$.[5] Despite such structural confusion, $NaNbO_3$ is well documented as being antiferroelectric at room temperature and, as a result of work presented by Shuvaeva et al., it is known to undergo an electric field induced phase

[†] University of St. Andrews.
[‡] Diamond Light Source Ltd.
[§] Rutherford Appleton Laboratory.

(1) Cross, E. *Nature* **2004**, *432*, 24.
(2) Saito, Y.; Takao, H.; Tani, T.; Nonoyama, T.; Takatori, K.; Homma, T.; Nagaya, T.; Nakamura, M. *Nature* **2004**, *432*, 84.
(3) Shuvaeva, V. A.; Antipin, M. Yu. *Crystallogr. Rep.* **1995**, *40*, 466.
(4) Glazer, A. M.; Megaw, H. D. *Acta Crystallogr.* **1973**, *A29*, 489.
(5) Darlington, C. N. W.; Knight, K. S. *Physica B* **1999**, *266*, 368.
(6) Darlington, C. N. W.; Knight, K. S. *Acta Crystallogr.* **1999**, *B55*, 24.
(7) Sakowski-Cowley, A. C.; Lukaszewicz, K.; Megaw, H. D. *Acta Crystallogr.* **1969**, *B25*, 851.
(8) Mishra, S. K.; Choudhury, N.; Chaplot, S. L.; Krishna, P. S. R.; Mittal, R. *Phys. Rev. B* **2007**, *76*, 024110.
(9) Modeshia, D. R.; Darton, R. J.; Ashbrook, S. E.; Walton, R. I. *Chem. Commun.* **2009**, 68.
(10) Shiratori, Y.; Magrez, A.; Dornseiffer, J.; Haegel, F.-H.; Pithan, C.; Waser, R. *J. Phys. Chem. B* **2005**, *109*, 20122.
(11) Megaw, H. D. *Proc. Phys. Soc.* **1946**, *58*, 133.

 10.1021/ja101860r © **2010 American Chemical Society**

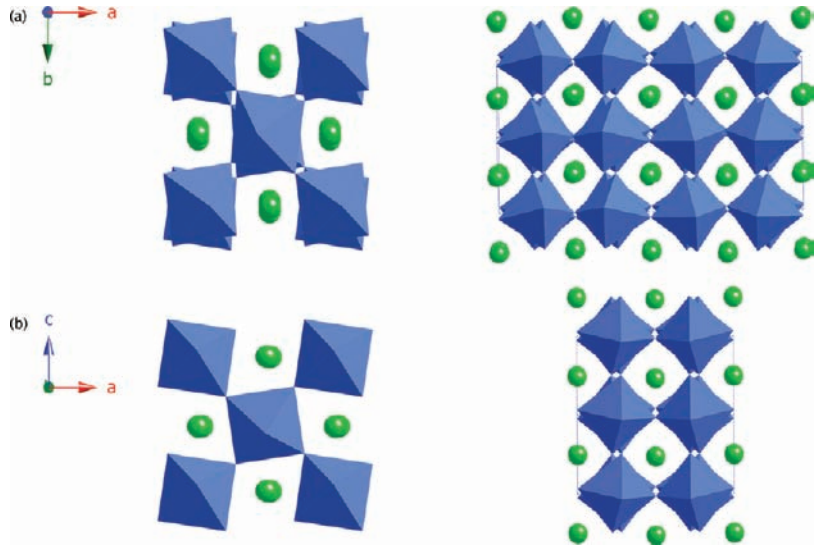

Figure 1. Crystal structures reported for the polymorphs (a) *Pbcm* and (b) $P2_1ma$ of $NaNbO_3$. Green spheres represent the sodium atoms, and the NbO_6 octahedra are shown as enclosed units (blue). Crystallographic data are taken from the literature.[7,12]

transition to a ferroelectric phase, in the polar space group $P2_1ma$, with unit cell dimensions $a = 5.569$ Å, $b = 7.790$ Å, and $c = 5.518$ Å.[12] In contrast to the *Pbcm* polymorph, the $P2_1ma$ polymorph exhibits a simpler octahedral tilt system leading to a smaller unit cell described by $\sqrt{2}a_p \times \sqrt{2}a_p \times 2a_p$, as shown in Figure 1b. This phase results from the polarization of single crystals of $NaNbO_3$.

Among the various structural studies undertaken on polycrystalline samples, submicrometer powders, and single crystals of $NaNbO_3$, Waser and co-workers[10,13] have suggested, based on X-ray powder diffraction and Raman spectroscopy, that samples of $NaNbO_3$ reveal a number of structural phase transitions as a function of particle size. One of the most interesting proposals is that $NaNbO_3$ crystallizes in the polar (and hence potentially ferroelectric) space group $Pmc2_1$ (alternative setting $P2_1ma$) at submicrometer particle sizes. This phase apparently corresponds to the "field-induced" phase of Shuvaeva.[12] Many of the ambiguities in determining the exact nature of the various $NaNbO_3$ polymorphs arise from the subtleties in the different octahedral tilting schemes well-known in perovskites. Octahedral tilting is an intrinsic property of perovskites and is a direct consequence of the relative sizes and nature of the A- and B-site cations. Glazer developed a convenient notation to describe the most commonly encountered tilt systems.[14,15] Owing to the ambiguities regarding the correct structural models for the various polymorphs of $NaNbO_3$, a variety of Glazer systems have been proposed. Subtle changes of this nature can be extremely difficult to detect using diffraction methods alone, and for this reason techniques that probe short-range order are highly beneficial because they enable local changes in the cation environments, particularly the A-sites, to be monitored closely. Moreover, given the confusion and apparent complexity surrounding the proposed ambient temperature polymorphs of $NaNbO_3$, it is essential to employ a variety of complementary techniques in order to establish their nature and how their occurrence depends on synthetic variables, particle size, temperature, and other intrinsic and extrinsic effects.

Here we present a comprehensive structural study of $NaNbO_3$ at room temperature using a variety of complementary techniques, including high-resolution X-ray (PXRD) and neutron powder diffraction (NPD), high-resolution solid-state ^{23}Na and ^{93}Nb magic-angle spinning (MAS) NMR, density functional theory (DFT) calculations, scanning electron microscopy (SEM), and second harmonic generation (SHG) measurements. Previous studies of $NaNbO_3$ have often focused primarily on the use of PXRD and NPD as methods for structural characterization. In contrast, there have been relatively few investigations using solid-state NMR,[16,17] the most detailed of which was by Ashbrook et al.[17] There has been a growing interest in the use of DFT calculations to aid assignment and interpretation of NMR spectra that has accelerated in recent years owing to the advancement and modification of computational codes. In particular, the introduction of codes that exploit the inherent periodicity and translational symmetry of solids has made them an integral addition to the solid-state NMR community, and a variety of applications investigating structure, order, and dynamics in a range of materials have been demonstrated.[18] Calculations provide a relatively easy way to monitor the variation of the NMR parameters with changes to local coordination environment, providing key assistance in the structural characterization of many solids, in this case $NaNbO_3$. In an effort to

(12) Shuvaeva, V. A.; Antipin, M. Yu.; Lindeman, S. V.; Fesenko, O. E.; Smotrakov, V. G.; Struchkov, Yu. T. *Ferroelectrics* **1993**, *141*, 307.
(13) Shiratori, Y.; Magrez, A.; Fischer, W.; Pithan, C.; Waser, R. *J. Phys. Chem. C* **2007**, *111*, 18493.
(14) Glazer, A. M. *Acta Crystallogr.* **1972**, *B28*, 3384.
(15) Woodward, P. M. *Acta Crystallogr.* **1997**, *B53*, 32.
(16) Wolf, F; Kline, D; Story, H. S. *J. Chem. Phys.* **1970**, *53*, 3538.
(17) Ashbrook, S. E.; Le Polles, L.; Gautier, R.; Pickard, C. J.; Walton, R. I. *Phys. Chem. Chem. Phys.* **2006**, *8*, 3423.
(18) (a) Harris, R. K.; Joyce, S. A.; Pickard, C. J.; Cadars, S.; Emsley, L. *Phys. Chem. Chem. Phys.* **2006**, *8*, 137. (b) Griffin, J. M.; Wimperis, S.; Berry, A. J.; Pickard, C. J.; Ashbrook, S. E. *J. Phys. Chem. C* **2009**, *113*, 465. (c) Ashbrook, S. E.; Berry, A. J.; Frost, D. J.; Gregorovic, A.; Pickard, C. J.; Readman, J. E.; Wimperis, S. *J. Am. Chem. Soc.* **2007**, *129*, 13213. (d) Pourpoint, F.; Gervais, C.; Bonhomme-Coury, L.; Azais, T.; Coelho, C.; Mauri, F.; Alonso, B.; Babonneau, F.; Bonhomme, C. *App. Magn. Reson.* **2007**, *32*, 435. (e) O'Dell, L.; Schurko, R. W. *Phys. Chem. Chem. Phys.* **2009**, *11*, 7069. (f) Chapman, R. P.; Bryce, D. *Phys. Chem. Chem. Phys.* **2009**, *11*, 6987. (g) Pallister, P. J.; Moudrakovski, I. L.; Ripmeester, J. A. *Phys. Chem. Chem. Phys.* **2009**, *11*, 11487. (h) Reader, S. W.; Mitchell, M. R.; Johnston, K. E.; Pickard, C. J.; Whittle, K. R.; Ashbrook, S. E. *J. Phys. Chem. C* **2009**, *113*, 18874.

gain an understanding of the relationship between structure and synthetic route, a variety of different synthesis methods have also been heavily investigated. Within this work, conventional solid-state techniques[19,20] are compared with molten salt[21] and sol-gel[22] approaches and significant differences are observed in the relative phases formed, as well as in both crystallinity and crystal morphology, thereby implying that synthesis route heavily influences both crystal structure and microstructure.

In particular, we report, unambiguously, the synthesis of a polar phase of $NaNbO_3$, possessing a pseudo-orthorhombic (probably, very subtly monoclinic: see later discussion) unit cell with dimensions $a = 5.571$ Å, $b = 7.766$ Å, and $c = 5.513$ Å and space group $P2_1ma$, and its characterization by a variety of methods. The relationship of this phase to those previously reported, in particular the electric field induced phase and "submicrometer" phase of Waser, is discussed. We also confirm that the original assignment of space group *Pbcm* to the commonly reported antiferroelectric polymorph is correct, and we show that suggestions of symmetry lowering to monoclinic in this phase can be explained by the presence of mixtures of the *Pbcm* and "$P2_1ma$" polymorphs.

Experimental Section

Synthesis. A sample of $NaNbO_3$ was purchased from Sigma-Aldrich (99.9%) and used without further purification. All other $NaNbO_3$ samples were synthesized using conventional solid-state, molten salt, and sol-gel methods. Using a solid-state approach, stoichiometric amounts of purchased Na_2CO_3 (Fisher Scientific, 99.5%) and Nb_2O_5 (Sigma-Aldrich, 99.99%) were mixed and ground in an agate mortar and pestle. Samples were pressed into 1 cm pellets, using a pressure of 10 tons cm^{-2}, and sintered at temperatures ranging from 450 to 950 °C for up to 48 h (Solid-State Samples A and B).[19,20] Excess Na_2CO_3 (~1−10%) was also added to a number of the solid-state reactions in an attempt to reduce the volatilization of the Na (Solid-State Sample C). In addition, different cooling rates were tested: slow cooling and quenching techniques were compared. Using the molten salt method, stoichiometric amounts of purchased Na_2O (Sigma-Aldrich, 80%) and Nb_2O_5 were ground and mixed with a quantity of NaCl equal to the total amount of reagents added and annealed at temperatures ranging from 850 to 1100 °C for 3−48 h. Once fully cooled, samples were washed in distilled H_2O, filtered, and allowed to air-dry at room temperature.[21] Using a sol-gel process, sodium ethoxide (3.67 mmol) and niobium(V) ethoxide (2.99 mmol) were dissolved in 2-methoxyethanol (10 mL) and refluxed at 80 °C for 90 min and then at 120 °C for an additional 90 min. Once fully heated, the solution was allowed to cool and the resultant product was sintered at 950 °C for 12 h.[22]

X-ray and Neutron Powder Diffraction. Room temperature "laboratory" powder X-ray diffraction (l-PXRD) experiments were carried out on a Stoe STADI-P X-ray diffractometer using Cu $K_{\alpha 1}$ ($\lambda = 1.540\,56$ Å) radiation. Using beamline I11 at the Diamond Light Source Synchrotron ($\lambda = 0.827\,267$ Å), high-resolution room temperature powder X-ray diffraction (s-PXRD) experiments were conducted.[23,24] Room temperature time-of-flight neutron powder diffraction (NPD) experiments were completed using the high resolution powder diffractometer (HRPD) at the ISIS neutron spallation source, Rutherford Appleton Laboratories. All diffraction data were analyzed by Rietveld refinement using the General Structure Analysis System (GSAS) software package.[25] Parameters refined included background coefficients, detector zero point, instrumental parameters, lattice parameters, profile coefficients, isotropic thermal factors, and atomic positional coordinates. An absorption correction was also applied to the neutron diffraction data. Further details of each refinement are given in Supporting Information.

NMR Spectroscopy. Solid-state NMR spectra were acquired using either a Bruker 400 or 600 Avance III spectrometer, equipped with wide-bore 9.4 or 14.1 T magnet, respectively, using Larmor frequencies of 105.8 and 158.75 MHz for ^{23}Na ($I = {}^3/_2$) and 146.89 MHz for ^{93}Nb ($I = {}^9/_2$). The finely powdered samples were tightly packed into conventional 4 and 2.5 mm ZrO_2 rotors, and magic-angle spinning (MAS) rates of 14 and 30 kHz, respectively, were employed. Chemical shifts were referenced to 1 M NaCl (aq) and a saturated solution of $K[NbCl_6]$ in acetonitrile, using NaCl (s) ($\delta_{iso} = 7.8$ ppm) and $LiNbO_3$ (s) (center of gravity of MAS line shape at $\delta = -1036.4$ ppm at 14.1 T) as secondary references. Conventional ^{23}Na and ^{93}Nb MAS NMR spectra were obtained using single pulse experiments at 14.1 T with typical (central-transition-selective) pulse lengths of 1.1 and 0.65 μs, respectively. Optimized recycle intervals for ^{23}Na and ^{93}Nb were 3 and 0.5 s. Typical radiofrequency field strengths employed were between 100 and 170 kHz. Two-dimensional triple-quantum MAS NMR experiments were recorded at 9.4 and 14.1 T using a phase-modulated rotor-synchronized split-t_1 shifted echo pulse sequence.[26] At 9.4 T spectra result from the averaging of 192 transients with a recycle interval of 3 s for each of the 98 t_1 increments of 126.98 μs, while at 14.1 T spectra result from the averaging of 96 transients with a recycle interval of 3 s for each of the 128 t_1 increments of 126.98 μs. ^{93}Nb MQMAS NMR spectra result from the averaging of 1440 transients with a recycle interval of 0.5 s for each of the 48 t_1 increments of 117.6 μs; an additional SPAM (soft-pulse added mixing)[27,28] pulse was added (resulting in a signal enhancement of ~40%). Chemical shift scales are referenced according to the convention in ref 29. Further experimental details can be found in the relevant figure captions. Additional ^{23}Na NMR data are also presented in the Supporting Information. Spectral analysis and fitting were performed within Topspin 2.1.

Calculations. ^{23}Na density functional theory (DFT) calculations were completed using the CASTEP[30] code, a planewave pseudopotential method that utilizes the gauge-including projector augmented wave (GIPAW) formalism. Calculations use the GGA PBE functional with ultrasoft pseudopotentials and periodic boundary conditions. Calculations were converged as far as possible with respect to k-point spacing and cutoff energy, with typical values of 0.04 $Å^{-1}$ and 60 Ry, respectively. Crystal structures were obtained from both the Inorganic Crystal Structure Database and Rietveld refinement of experimental data. Where necessary, geometry optimization of the structure was performed prior to calculation of the NMR parameters. Calculations output both the absolute shielding tensor and the electric field gradient (EFG) tensor in the crystal frame. The isotropic chemical shift, δ_{iso}, can be obtained from the isotropic shielding, σ_{iso}, by

$$\delta_{iso} = -(\sigma_{iso} - \sigma_{ref})$$

(19) Castro, A.; Jimenez, B.; Hungria, T. *J. Eur. Ceram. Soc.* **2004**, *24*, 941.
(20) Wu, L.; Zhang, J.; Wang, C.; Li, J. *J. Appl. Phys.* **2008**, *103*, 084116.
(21) Arendt, R.; Rosolowski, J. Molten Salt Synthesis of Alkali Niobate Powders. U.S. Patent 4234557, 1980.
(22) Tanaka, K.; Kakimoto, K.; Ohsato, H. *J. Eur. Ceram. Soc.* **2007**, *27*, 3591.
(23) Tang, C. C.; Thompson, S. P.; Hill, T. P.; Wilkin, G. R.; Wagner, U. H. *Z. Kristallogr. Suppl.* **2007**, *26*, 153.
(24) Thompson, S. P.; Parker, J. E.; Potter, J; Hill, T. P.; Birt, A.; Cobb, T. M.; Yuan, F.; Tang, C. C. *Rev. Sci. Instrum.* **2009**, *80*, 075107.
(25) Larson, A. C.; von Dreele, R. B. Report No. LA-UR-86-748; Los Alamos National Laboratory: Los Alamos, NM, 1987.
(26) Brown, S. P.; Wimperis, S. *J. Magn. Reson.* **1997**, *124*, 279.
(27) Gan, Z.; Kwak, H. *J. Magn. Reson.* **2004**, *168*, 346.
(28) Ball, T. J.; Wimperis, S. *J. Magn. Reson.* **2007**, *187*, 343.
(29) Pike, K. J.; Malde, R. P.; Ashbrook, S. E.; McManus, J.; Wimperis, S. *Solid State Nucl. Magn. Reson.* **2000**, *16*, 103.
(30) Clark, S. J.; Segall, M. D.; Pickard, C. J.; Hasnip, P. J.; Probert, M. J.; Refson, K.; Payne, M. C. *Z. Kristallogr.* **2005**, *220*, 567.

where σ_{ref} is the reference isotropic shielding (565.84 ppm for ^{23}Na), determined from calculations on the ilmenite polymorph of $NaNbO_3$.[9] The quadrupolar interaction is characterized by a magnitude, C_Q, and asymmetry, η_Q, derived from the principal components of the EFG tensor:

$$C_Q = eQV_{ZZ}/h$$

$$\eta_Q = (V_{XX} - V_{YY})/V_{ZZ}$$

where $|V_{ZZ}| \geq |V_{YY}| \geq |V_{XX}|$ and Q is the nuclear electric quadrupole moment. For ^{23}Na and ^{93}Nb, Q is 104 and -320 mb, respectively.[31] The quadrupolar product, P_Q, is also routinely used and is given by

$$P_Q = C_Q(1 + \eta_Q^2/3)^{1/2}$$

All calculations were performed on the EaStCHEM Research Computing Facility, consisting of 152 AMD Opteron processing cores partly connected by Infinipath high speed interconnects. Typical calculation times were up to 24 h using 12 cores.

Second Harmonic Generation (SHG). Nonlinear optic (NLO) properties were studied using powder second harmonic generation (SHG) techniques. Samples were pressed between two microscope slides and analyzed using a Nd vanadate pulsed laser. Each pulse had a typical duration of 12 ps. Pulses typically came in bundles of 2−5 and at a rate of 1 kHz. The beam diameter was 5 mm, and the power used varied between 1 and 2.5 W.

Scanning Electron Microscopy (SEM). The crystal morphology of each sample was examined using scanning electron microscopy (SEM) on a Jeol JSM-5600 microscope operating at 20−30 kV equipped with an Oxford INCA system for energy-dispersive X-ray spectroscopy (EDX).

Results and Discussion

Commercial Sample. Initial investigations concentrated on $NaNbO_3$ purchased commercially (Sigma-Aldrich). Structure and phase purity were initially verified using l-PXRD and then s-PXRD, both of which displayed excellent agreement with the orthorhombic structure reported in the literature (*Pbcm*).[32] The Rietveld refinement using the s-PXRD data is shown in Figure 2a, and full refinement details can be found in Supporting Information. The ^{23}Na MAS NMR spectrum (Figure 2b) contains a broadened line shape, hindering the extraction of information regarding the number of crystallographically distinct Na sites present. ^{23}Na ($I = {}^3/_2$) is a quadrupolar nucleus, and under conventional MAS, ^{23}Na line shapes commonly exhibit broadening as a result of the inefficient removal of second-order quadrupolar interactions. For this reason high-resolution NMR techniques such as multiple-quantum MAS[33] (MQMAS) are required to fully remove inhomogeneous second-order quadrupolar broadenings and resolve distinct sites. The ^{23}Na triple-quantum MAS spectrum of $NaNbO_3$, shown in Figure 2b, clearly displays two distinct Na resonances, in agreement with the reported crystal structure for *Pbcm* $NaNbO_3$.[32] The projection of the spectrum onto the δ_1 axis also exhibits two sharp isotropic peaks, again highlighting the presence of two distinct Na environments. From MQMAS spectra it is possible to extract information regarding both quadrupolar and chemical shift interactions in a number of ways. From the position of the center of gravity of the ridge line shape (δ_1, δ_2), the isotropic chemical shift, δ_{iso}, and the quadrupolar product, P_Q can be determined. Alternatively, the parameters δ_{iso}, C_Q, and the asymmetry, η_Q, may be obtained by computer fitting of an extracted cross-section, parallel to δ_2. However, the line shape obtained in this case can be distorted as a result of nonuniform excitation and conversion of triple-quantum coherences.[34] The NMR parameters extracted from the spectra in Figure 2 are given in Table 1. The upper and notably narrower of the two ridges in the two-dimensional spectrum, with $\delta_{iso} = -4.2$ ppm, has $P_Q = 1.2$ MHz, while the lower ridge, with $\delta_{iso} = -0.6$ ppm, has a considerably larger quadrupolar contribution, $P_Q = 2.2$ MHz. It is possible to confirm the accuracy of the parameters extracted by simulating the MAS spectrum that would result. This is shown in the Supporting Information and is in good agreement with that obtained experimentally. ^{93}Nb ($I = {}^9/_2$) is also a quadrupolar nucleus, and the MAS NMR spectrum obtained (Figure 2c) exhibits features characteristic of the second-order quadrupolar interaction, although a small additional broadening appears to be present. The ^{93}Nb MQMAS spectrum confirms the presence of a single Nb resonance, although additional broadening is observed here also, suggesting the presence of some disorder. The NMR parameters extracted from the spectrum in Figure 2c are given in Table 1 and are in good agreement with the literature.[35,36]

Solid-State Preparation. $NaNbO_3$ was also synthesized using conventional solid-state techniques (Solid-State Sample A). Phase purity was examined using PXRD and displayed good agreement with the literature, initially suggesting the presence of single-phase *Pbcm* $NaNbO_3$, as shown in Figure 3a. However, under MAS the ^{23}Na NMR spectrum appears different in comparison to that obtained for the commercially purchased sample, as shown in Figure 4a and Figure 4b. In addition, the crystallinity and microstructure displayed visible differences (Figure 4g and Figure 4h). Using ^{23}Na MQMAS NMR, however, it was evident a second Na-containing phase was present in Solid-State Sample A. At 14.1 T an additional resonance was clearly observed at $\delta_1 = -9.3$ ppm, as shown in Figure 5a. In addition, the resonance at $\delta_1 = 4.3$ ppm covers a wider δ_2 shift range, suggesting the potential overlap of two resonances here also. This is highlighted in the overlay of the ^{23}Na MQMAS NMR spectra for this sample and that of the commercial material shown in the Supporting Information. Therefore, in an attempt to resolve any overlapped sites an MQMAS spectrum was recorded at 9.4 T. The position of resonance in an isotropic MQMAS spectrum depends not only on the chemical shift but also on the quadrupolar interaction, and owing to the differing field dependences of these interactions (proportional to B_0 and B_0^{-1}, respectively), resolution may be improved at both lower and higher magnetic field strength. As shown in Figure 5b, four crystallographically distinct Na sites are clearly observed, suggesting the presence of a second Na-containing phase, with two Na species. Although the intensity of resonances in MQMAS spectra is in general nonquantitative (i.e., does not accurately reflect the proportions of different phases), for species with very similar quadrupolar interactions it is possible to interpret spectral intensities in a quantitative way. The two peaks

(31) Pyykko, P. *Mol. Phys.* **2008**, *106*, 1965.
(32) Chizhova, E. A.; Klyndyuk, A. I.; Bashkirov, L. A.; Petrov, G. S.; Makhnach, L. V. *Neorg. Mater.* **2004**, *40*, 1508.
(33) Frydman, L.; Harwood, J. S. *J. Am. Chem. Soc.* **1995**, *117*, 5367.
(34) Fernandez, C.; Amoureux, J. P. *Solid State Nucl. Magn. Reson.* **1996**, *5*, 315.
(35) MacKenzie, K. J. D.; Smith, M. E. *Multinuclear Solid-State NMR of Inorganic Materials*; Pergamon Materials Series, Vol. 6; Pergamon: Oxford, U.K., 2002; p 665.
(36) Hanna, J. V.; Pike, K. J.; Charpentier, T.; Kemp, T. F.; Smith, M. E.; Lucier, B. E. G.; Schurko, R. W.; Cahill, L. S. *Chem.—Eur. J.* **2010**, *16*, 3222.

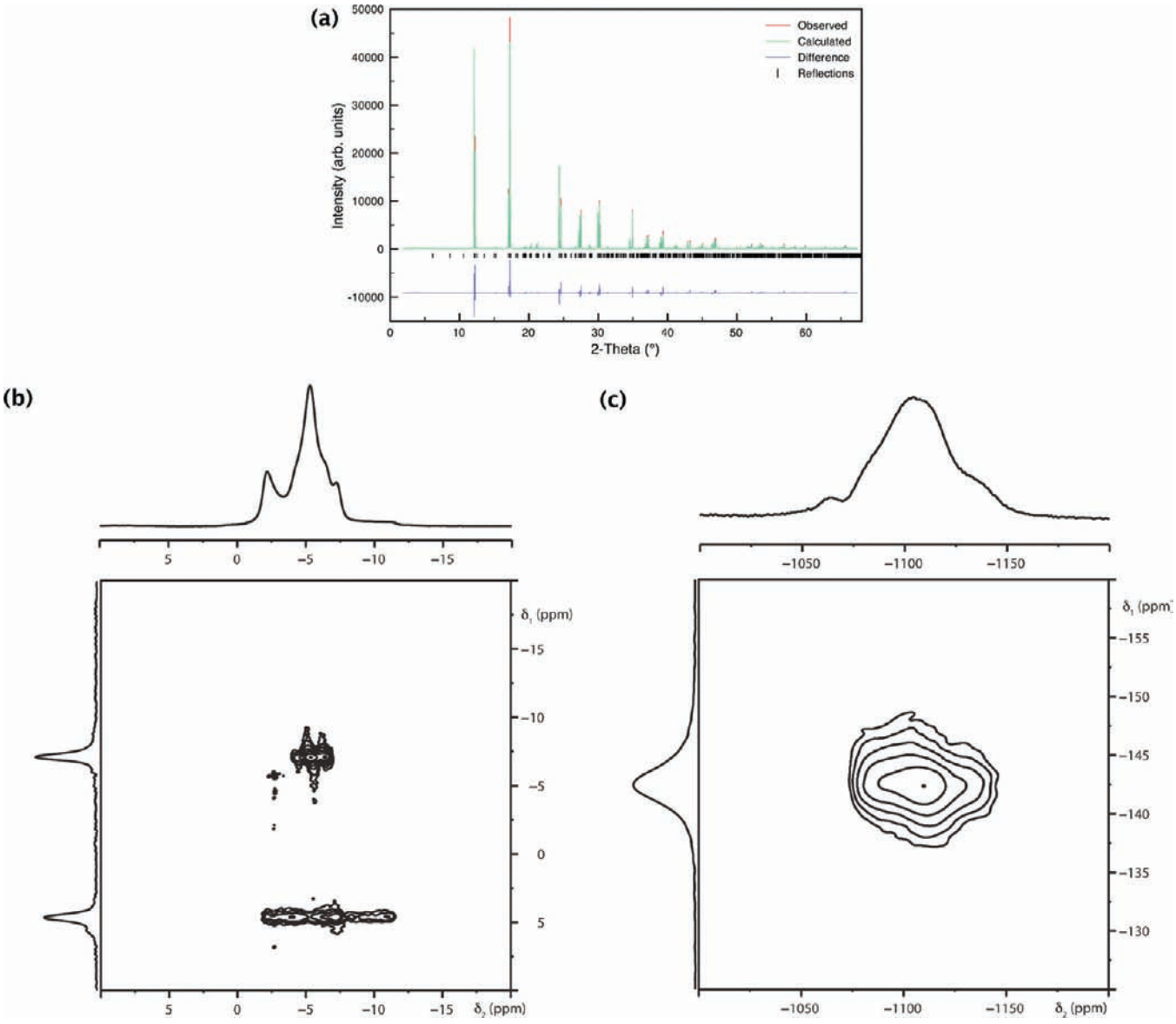

Figure 2. Commercial $NaNbO_3$ (Aldrich): (a) Rietveld profile (*Pbcm* model) of s-PXRD data; (b) conventional ^{23}Na (14.1 T) MAS NMR spectrum, triple-quantum MAS NMR spectrum, and corresponding isotropic projection; (c) conventional ^{93}Nb (14.1 T) MAS NMR spectrum, triple-quantum MAS NMR spectrum, and corresponding isotropic projection.

at $\delta_1 = -9.3$ and -7.5 ppm suggest that the second phase accounts for ~40% of the material synthesized in this case. NMR parameters extracted for each phase at 14.1 and 9.4 T are given in Table 1. Accurate quadrupolar parameters could not be extracted for all sites owing to spectral overlap and significant line broadening and distortion, potentially caused by either nonuniform triple-quantum excitation or positional disorder. Therefore, P_Q values derived from the position of the center of gravity have been quoted for these sites.

Using solid-state techniques, several additional samples were synthesized to determine whether the extra phase identified in Solid-State Sample A was consistently and repeatably produced in all samples synthesized using solid-state methods. Various experimental conditions were thoroughly investigated, including annealing temperature and time, the effects of different cooling rates (e.g., quenching vs slow cooling), and the effect of addition of an excess (1−10%) of the primary starting reagent Na_2CO_3. Using solely l-PXRD, Rietveld refinements were completed for all samples and initially suggested the presence of a single-phase perovskite in space group *Pbcm* (Rietveld refinements and refined lattice parameter values for Solid-State Samples B and C are located in Supporting Information). Again, using ^{23}Na MAS NMR, the lineshapes obtained displayed subtle variations when compared with the commercially purchased sample, suggesting a different composition within each (Figure 4a,c,d). This is perhaps more easily seen when the line shapes for these different phases are superimposed, as shown in the Supporting Information. Upon closer inspection using two-dimensional ^{23}Na MQMAS NMR, it was evident that the same secondary phase was consistently present, with two additional Na sites. Using variations of the original solid-state synthesis, it was possible to vary the quantities of each phase significantly, from as little as a few percent to almost a 50% mix of the two; however, the *Pbcm* phase was consistently present as the major phase, suggesting it to be the more thermodynamically stable of the two. It was possible to slightly reduce the quantity of the second phase by addition of a small excess of Na_2CO_3; however, it was never possible to fully eradicate it using such methods. In

Table 1. Experimental NMR Parameters, δ_{iso}, P_Q, C_Q, and η_Q, for Commercially Purchased $NaNbO_3$ (Aldrich), Solid-State Sample A $NaNbO_3$, and Sol-Gel $NaNbO_3$ Sample, Obtained from the MAS and MQMAS Spectra in Figures 2b, 5a,b, and 7c, Respectively

	site	δ_{iso} (ppm)	P_Q, MHz	C_Q, MHz	η_Q
		Commercial Sample (Aldrich)			
Pbcm	Na1	−0.6(5)	2.2(1)		
	Na2	−4.2(5)	1.2(2)		
	Nb1	−1078.3(5)	21.2(2)	19.6(2)	0.7(1)
		Solid-State Sample A (14.1 T)			
Pbcm	Na1	−0.7(5)	2.2(1)		
	Na2	−4.4(5)	1.2(2)		
"$P2_1ma$"	Na1	−5.1(5)	1.1(2)		
		Solid-State Sample A (9.4 T)			
Pbcm	Na1	−0.5(5)	2.1(1)	2.1(1)	0.0(1)
	Na2	−4.2(5)	1.2(2)	1.0(2)	0.8(1)
"$P2_1ma$"	Na1	−1.4(5)	2.4(1)	2.1(1)	0.9(1)
	Na2	−5.1(5)	1.2(2)	1.1(2)	0.7(1)
		Sol-Gel Sample			
"$P2_1ma$"	Na1	−1.5(5)	2.4(1)		
	Na2	−5.1(5)	1.2(2)		

addition, there appears to be no real correlation between solid-state synthesis and the quantity of the second phase produced. All solid-state experimental conditions were tested multiple times to establish the feasibility of achieving reproducible results, all of which confirmed that it was not possible to routinely synthesize samples with identical ratios of the two phases. This suggests that solid-state synthesis is not an easily controlled experimental method and, in this particular case, it is presumably owing to the volatile nature of the Na-based starting reagents. Working with highly volatile materials can lead to a nonstoichiometric reaction mixture, resulting in incomplete reaction or, more commonly, the formation of unknown intermediate phases. It is also extremely difficult to ensure complete mixing of the powdered starting reagents; therefore, to overcome this, the precursors are often mixed in a solvent (commonly acetone or ethanol) prior to reaction at high annealing temperatures. This reduces particle size and ensures complete mixing of the powders. In contrast to sol-gel techniques, solid-state methods commonly produce samples with reasonably good crystallinity. This is highlighted in Figure 4h−j in which partially formed cubelike microstructures are observed for Solid-State Samples A and C. To obtain highly crystalline samples, a relatively slow rate of reaction is required.

The sample containing the largest quantity of the second phase (∼50%), Solid-State Sample A, was analyzed in more detail. Using l-PXRD, it was virtually impossible to identify any significant differences between this and that of phase pure *Pbcm* $NaNbO_3$, indicating the two phases must be, structurally, very closely related. X-ray diffraction principally examines the long-range order within a material, whereas solid-state NMR investigates more local, short-range effects. The two techniques are therefore highly complementary to one another and enable enhanced structural characterization of many complex solids. For the case of $NaNbO_3$, solid-state NMR provides more detailed information regarding the number of crystallographically distinct Na sites present and, in turn, the number of phases. NMR identifies the presence of two highly crystalline phases, confirming that X-ray diffraction is not simply missing the identification of an amorphous phase. This, in turn, provides confirmation that both phases diffract in a similar manner producing peaks that essentially overlap, thereby suggesting the second phase to be a polymorph of $NaNbO_3$ rather than an impurity phase. Without high-resolution diffraction data, it is extremely challenging to distinguish between the two, with the only subtle visible discrepancies occurring in the superstructure peaks ($2\theta = 34-42°$), as shown in Figure 3b. However, solid-state NMR generally does not provide detailed information regarding the symmetry adopted within a structure or the precise location of the oxygen or sodium positions. To obtain this detailed information, diffraction is a necessity. Neutron diffraction is therefore essential for the study of $NaNbO_3$ because it enhances superstructure peaks and enables accurate location of the oxygen atoms, which ultimately aids in structural refinement and, in turn, spectral interpretation. Hence, both high-resolution synchrotron X-ray and neutron powder diffraction were undertaken on Solid-State Sample A.

The high-resolution diffraction data collected for Solid-State Sample A were analyzed in significant detail, and single phase refinements were completed for both data sets using the *Pbcm* model[32] (refined lattice parameter values are located in Supporting Information). It was immediately apparent in both data sets that a single model was insufficient owing to considerable discrepancies between the theoretical model and experimental data. The Rietveld refinement completed using the s-PXRD data (Figure 3c) highlighted regions in which shoulders and/or peaks were unaccounted for. Upon closer inspection it was evident split peaks were not indexed by the model and the lattice parameters considered them simply as single peaks. In addition, a number of the most intense peaks were not allocated sufficient intensity by the model, leading to relatively poor agreement factor, wRp (24.5%) and χ^2 (23.0) values. The Rietveld refinement completed using the NPD data was significantly more informative and is shown in Figure 3e. Neutron diffraction enhances superstructure peaks; therefore, the small discrepancies initially identified by l-PXRD were magnified considerably by neutrons. The quality of refinement produced using solely the conventional *Pbcm* model was relatively poor (wRp = 13.8% and χ^2 = 61.1), in particular over lower *d*-spacings. More specifically, two peaks in the experimental data at 2.47 and 2.49 Å were not accounted for in the model, suggesting they were associated with the additional polymorph present. These peaks are highlighted in Figure 3f. Using this in conjunction with the ^{23}Na NMR data, it was obvious a second phase very closely related to the orthorhombic *Pbcm* phase was present. A more detailed discussion of the possibility of multiphase refinements for Solid-State Sample A is given later.

Molten Salt Preparation. Initially, the precise experimental conditions required to synthesize a sample of $NaNbO_3$ using molten salt techniques were unknown; therefore, several "test" reactions were undertaken to establish feasible reaction conditions. Using an annealing temperature of 850 °C for 24 h, a sample of $NaNbO_3$ was synthesized. Phase purity was verified using PXRD, and Rietveld refinement confirmed that the sample refined well to the orthorhombic structure, *Pbcm*. EDX analysis revealed no presence of residual Cl^- from the synthesis (see Supporting Information for details of these spectra). ^{23}Na MAS NMR again produced a broadened line shape that appeared subtly different from the commercially purchased sample (Figure 4a and Figure 4e). (These two line shapes are shown overlaid in the Supporting Information.) This, in turn, failed to provide adequate information regarding both the composition of the sample and number of crystallographically distinct Na sites present; hence, MQMAS techniques were utilized. The triple-quantum ^{23}Na MQMAS spectrum indicated the presence of a second Na-containing phase, as observed for materials synthesized using solid-state methods (see Figures 5 and 6). The

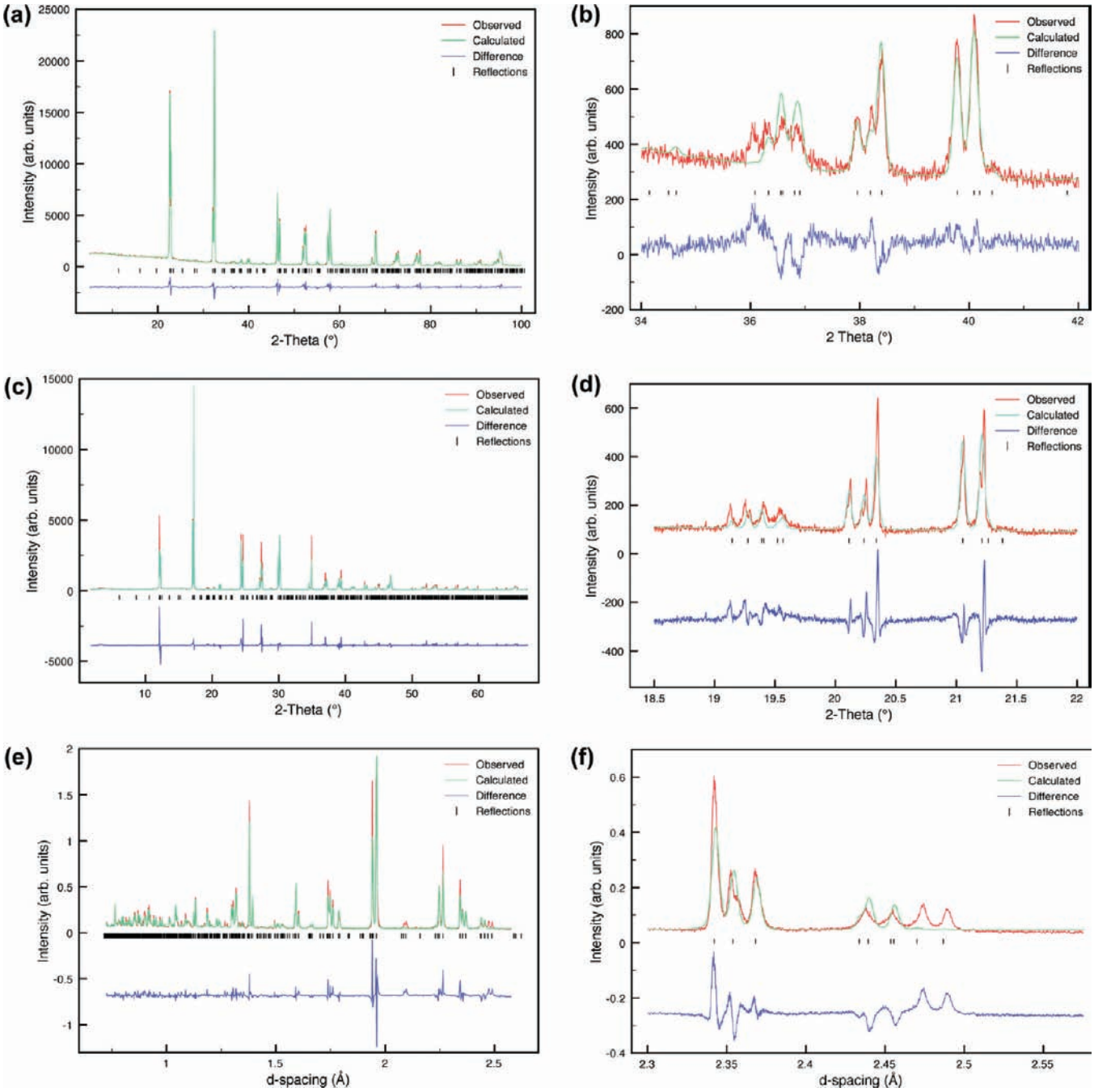

Figure 3. Rietveld profiles for Solid-State Sample A $NaNbO_3$, *Pbcm* model: (a, b) l-PXRD data; (c, d) s-PXRD data; (e, f) high-resolution NPD data. Expansions of the corresponding superstructure peaks are shown in (b) ($2\theta = 34-42°$), (d) ($2\theta = 18.5-22°$), and (f) (2.3−2.55 Å). Note that the different 2θ range presented is due to the different wavelengths used for the l- and s-PXRD measurements.

isotropic spectrum indicated the quantity of this phase to be considerably reduced (to ∼1−5%) when compared with the samples prepared using solid-state synthesis. Such a result suggested this synthetic method to be the most promising way of significantly reducing the phase or even eradicating it completely. Therefore, using this approach, a systematic study of annealing temperature and time was completed to determine the effect on the quantity of second phase produced. Samples synthesized using this method possessed morphological uniformity, most probably owing to intimate mixing of the starting reagents due to reaction in a liquid medium. In particular, samples synthesized using an annealing temperature of 1000 °C for 24 h produced crystallites with almost fully formed cubelike microstructures, shown in Figure 4k. Initially, temperature was the sole variable, investigating the range between 850 and 1100 °C with annealing times fixed at 24 h. Using Rietveld refinement, all PXRD data in this range refined well to the *Pbcm* model. However, two-dimensional ^{23}Na NMR data highlighted the presence of an additional phase that consistently correlated with that identified in the initial molten salt sample synthesized. Via a systematic temperature study, it was possible to eliminate this secondary phase entirely using a temperature of 1000 °C, as shown in Figure 6a. However, at higher temperatures a reduction in crystallinity was observed. In addition, heating times between 3 and 48 h were tested on reactions using 1000 °C. Rietveld refinement of all samples

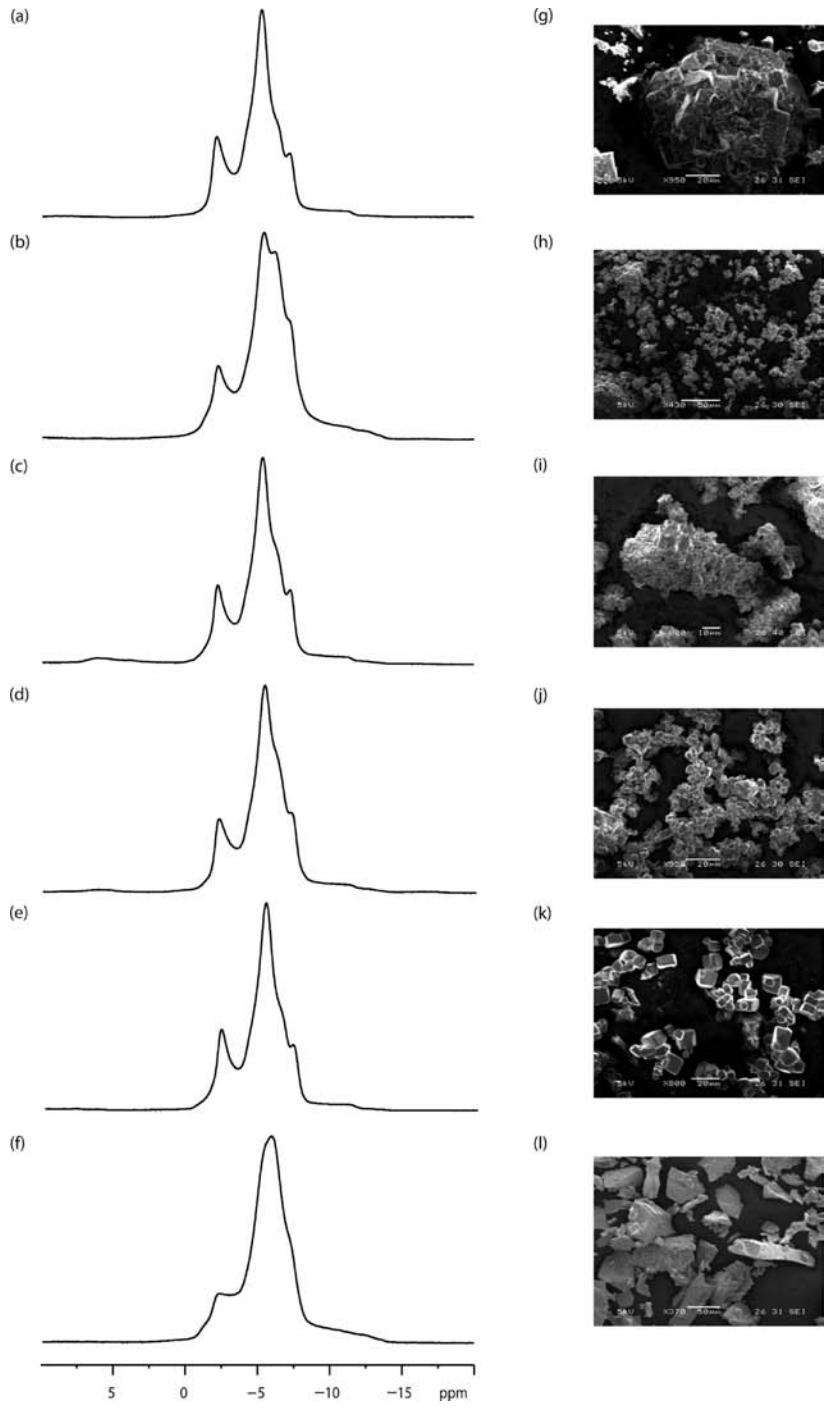

Figure 4. Comparison of (a−f) ^{23}Na (14.1 T) MAS NMR spectra and (g−l) scanning electron microscopy (SEM) images of (a, g) commercially purchased $NaNbO_3$ (Aldrich), (b, h) Solid-State Sample A $NaNbO_3$, (c, i) Solid-State Sample B $NaNbO_3$, (d, j) Solid-State Sample C $NaNbO_3$, (e, k) molten salt $NaNbO_3$ (850 °C for 24 h), and (f, l) sol-gel $NaNbO_3$.

indicated excellent agreement with the literature, again suggesting the presence of single phase *Pbcm* $NaNbO_3$, and once again, it was not possible to trace either the presence or quantity of any impurity phase using solely diffraction. Samples prepared using shorter reaction times displayed an abundance of the second phase previously identified in the temperature-dependent study; however, it was possible to eradicate the phase after 24 h of heating to leave solely the *Pbcm* phase of $NaNbO_3$. Samples with longer annealing times confirmed this trend, indicating that the second phase did not return to the sample and the phase produced was thermodynamically stable. Using ^{23}Na MQMAS, the presence and relative quantities of the second phase were easily observed as shown in the isotropic projections in Figure 6b. All Rietveld refinements and two-dimensional ^{23}Na NMR spectra for both heating series can be found in the Supporting Information.

Two phases are consistently synthesized using molten salt techniques; however, both temperature and time appear to affect the formation of the second phase. In the case of our molten salt reactions it is possible to determine the exact temperature and time of reaction required to fully eradicate the second phase. For solid-state reactions this does not seem to be the case. The synthetic conditions alter the proportions of the two phases present, but it is not possible to remove either entirely. Even

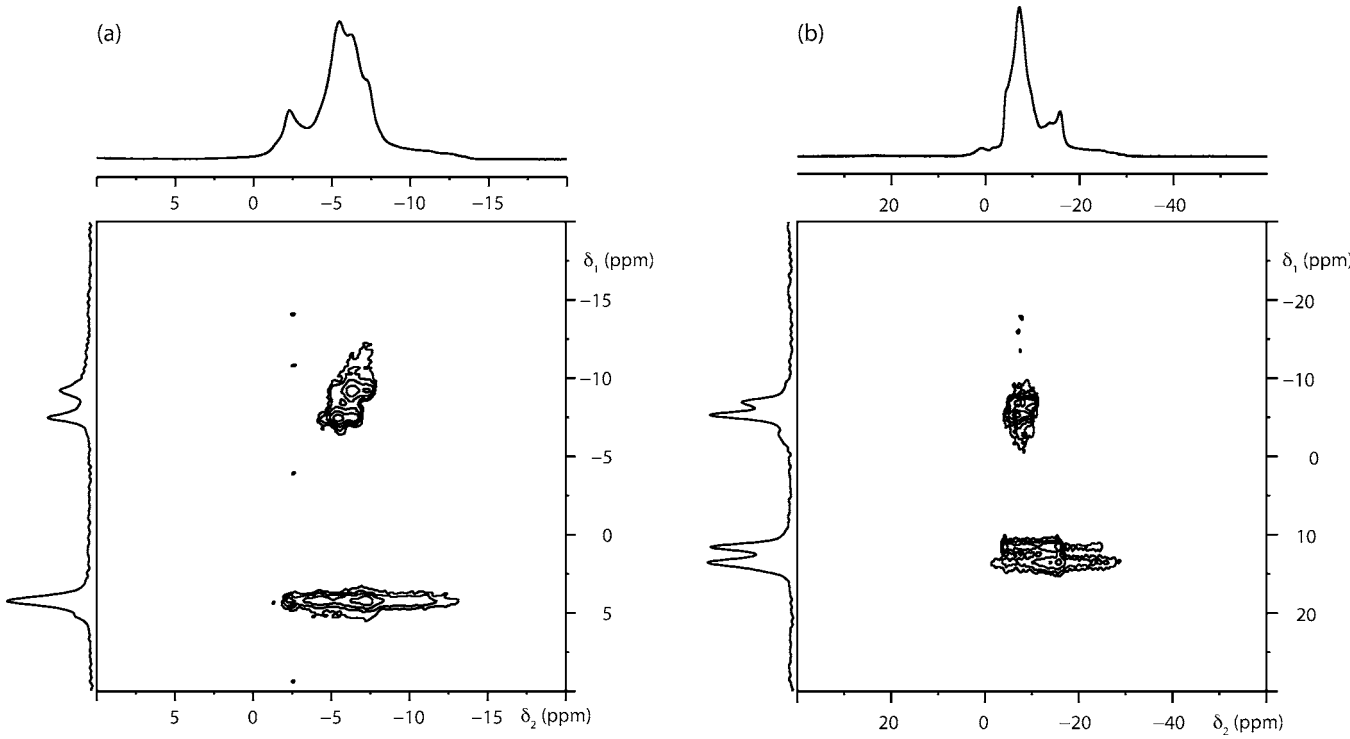

Figure 5. ^{23}Na MAS NMR spectra, triple-quantum MAS NMR spectra, and corresponding isotropic projections for Solid-State Sample A $NaNbO_3$ at (a) 14.1 T and (b) 9.4 T.

when reactions were carried out with apparently similar conditions, the proportions of the two phases obtained varied. In both solid-state and molten salt reactions the major polymorph formed was the *Pbcm* phase, although the proportion of the second phase was as high as ~40% in some solid-state syntheses. However, by means of a molten salt approach, it was possible to synthesize phase pure *Pbcm* $NaNbO_3$. Unfortunately, this provides little or no assistance in determining the precise nature of the second phase, although it does, however, provide valuable information regarding reaction mechanism. Using this approach, it was therefore possible to successfully trace the intergrowth of the unknown secondary phase in both heating series.

Sol-Gel Preparation. In order to use a diverse range of synthetic routes and to clarify the nature of the second polymorph present in the solid-state preparations, a sol-gel approach was also utilized. In a manner similar to molten salt techniques this allows intimate mixing and reaction of the starting reagents. Conventionally, solid-state methods are adopted over sol-gel processes for the synthesis of perovskites owing, principally, to the simplicity of the reaction. However, occasionally sol-gel methods are favored, as they can enable alternative phases to form that are not commonly observed within solid-state reactions. An associated disadvantage of these processes, particularly in the case of $NaNbO_3$, is the severe lack of control and reproducibility.

Using a basic sol-gel approach, a sample of $NaNbO_3$ was synthesized and structure and phase purity were studied using PXRD. It was immediately apparent that a polymorph of $NaNbO_3$ had been synthesized that was different from the commonly formed orthorhombic *Pbcm* phase. Rietveld refinement of l-PXRD data (Figure 7a) highlighted differences in the superstructure peaks ($2\theta = 34-42°$), as shown in Figure 7b, in which the theoretical model (*Pbcm*) placed intensity where no observed experimental data appeared. The presence of a different polymorphic form of $NaNbO_3$ was confirmed using synchrotron X-ray and neutron powder diffraction. Close examination of the high-resolution diffraction data revealed the disappearance of the peaks due to the $4a_p$ superlattice, thereby indicating that the phase present did not require additional doubling of the unit cell, as in *Pbcm*, merely the $\sqrt{2}a_p \times \sqrt{2}a_p \times 2a_p$ cell. This type of distortion in perovskites is well-known (in fact it corresponds to the most common tilt system $a^-a^-b^+$). A standard structural model for the centrosymmetric orthorhombic space group *Pnma* was sufficient to index all peaks, and each data set refined reasonably well to this model. Refinement details for the NPD data (using both isotropic and anisotropic temperature factors) can be found in the Supporting Information. Using conventional ^{23}Na MAS NMR, a different and broadened line shape was observed, which appeared to have lost many of the sharp, distinct features previously identified in the commercially purchased sample. This can be seen in Figure 4a,f and in the Supporting Information where the two line shapes are overlaid. Two-dimensional ^{23}Na MQMAS NMR also confirmed the presence of a different phase of $NaNbO_3$ in addition to a small percentage (~10%) of the *Pbcm* phase (Figure 7c). It was evident this new phase contained two crystallographically distinct Na sites with δ_1 values of -7.1 and 13.5 ppm, thereby contradicting the conclusions initially drawn from diffraction data alone. The NMR parameters extracted from this spectrum are given in Table 1. Although providing an adequate refinement to both the synchrotron and neutron data, the presence of only a single distinct Na species for *Pnma* reveals that it would not appear to be the correct model. In addition, when refined anisotropically, the oxygen atom O1 did not have a positive definite thermal displacement factor, thereby indicating this model to be incorrect. The Rietveld refinement of the sol-gel $NaNbO_3$ sample using *Pnma* can be found in Supporting Information.

Perovskites frequently favor centrosymmetric structures except when ferroelectric ions are present. Of the many reported

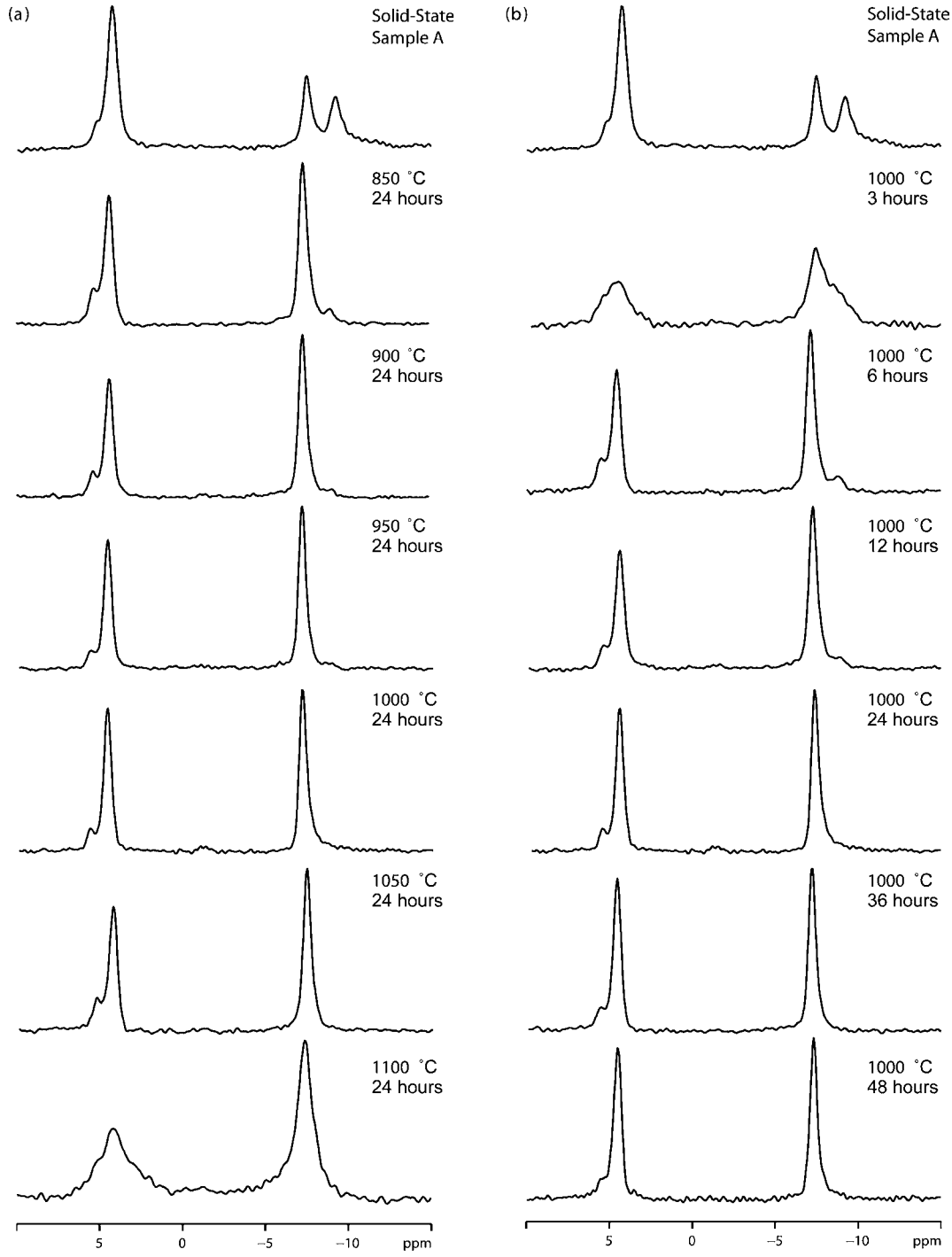

Figure 6. Isotropic projections obtained from triple-quantum ^{23}Na (14.1 T) MAS NMR spectra of molten salt samples of $NaNbO_3$. In (a), annealing temperature was varied from 850 to 1100 °C, with a fixed annealing time of 24 h. In (b), the annealing time was varied from 3 to 48 h, with a fixed annealing temperature of 1000 °C. For comparison the isotropic projection for Solid-State Sample A of $NaNbO_3$ is also shown.

polymorphs of $NaNbO_3$, most are centrosymmetric with only one confirmed report of a noncentrosymmetric structure, that by Shuvaeva et al.[12] Both the neutron and ^{23}Na NMR data presented suggested that the newly synthesized polymorph of $NaNbO_3$ had undergone a reduction in symmetry from the centrosymmetric space group *Pnma* to a noncentrosymmetric structure. Therefore, to provide further support for this, the nonlinear optic (NLO) properties of selected $NaNbO_3$ samples were tested. Second harmonic generation (SHG) experiments are a relatively simple and effective way of identifying whether a structure is centrosymmetric or noncentrosymmetric. SHG measurements were conducted on both the sol-gel sample and a phase pure sample of $NaNbO_3$ (synthesized using molten salt techniques). The sol-gel sample displayed an intense SHG active signal, thereby indicating it to be noncentrosymmetic. (Further details of these experiments can be found in the Supporting Information.) This, in conjunction with the ^{23}Na NMR data, provided a significant step toward structural characterization and allowed identification of three potential noncentrosymmetric subgroups of *Pnma*; $P2_1ma$, $Pn2_1a$, and $Pnm2_1$. Rietveld refinements were completed for each potential space group using the NPD data collected, although it should be noted that the

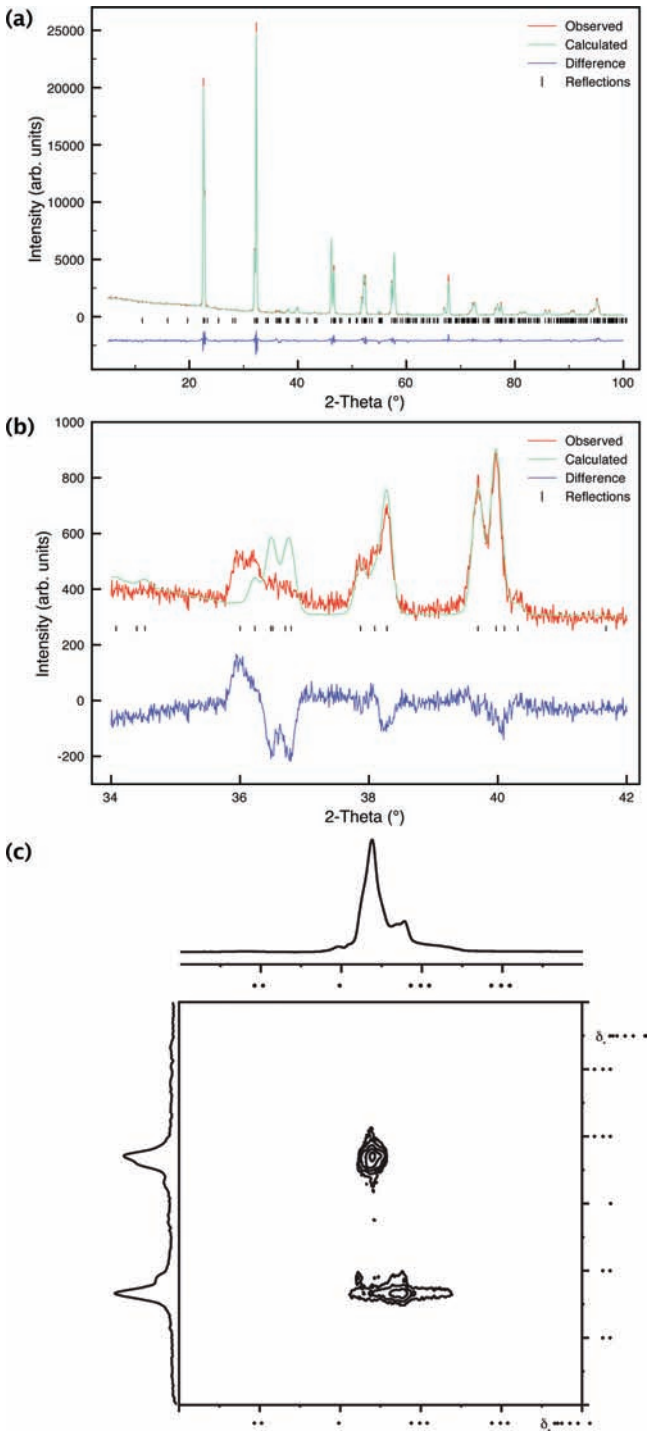

Figure 7. Sol-gel $NaNbO_3$: (a) Rietveld profile (*Pbcm* model) of l-PXRD data; (b) corresponding expansion of the superstructure peaks ($2\theta = 34-42°$) highlighting areas of discrepancy; (c) conventional ^{23}Na (9.4 T) MAS NMR spectrum, triple-quantum MAS NMR spectrum, and corresponding isotropic projection.

$Pn2_1a$ model also possesses only a single Na site. Interestingly, the work by Shuvaeva was the result of an electric field induced phase transition from *Pbcm* to $P2_1ma$ in a single crystal of $NaNbO_3$. This polymorph was also recently reported by Waser et al.,[10,13] as existing in submicrometer powders of $NaNbO_3$. Their work suggests that $NaNbO_3$ undergoes a particle size induced phase transition from *Pbcm* to *Pmma* via the orthorhombic phase $Pmc2_1$ (alternative setting $P2_1ma$). Using microemulsion-mediated synthetic techniques, nanosized powders were synthesized and annealed at various temperatures, producing a range of micrometer, submicrometer, and nano-ordered powders. In a later publication Waser et al. investigated similar temperature and pressure induced phase transitions for submicrometer powders of $NaNbO_3$ and identified a submicrometer sample similar to that previously synthesized. Using piezoresponse force microscopy (PFM), the sample was confirmed to be noncentrosymmetric and, in turn, suggested the presence of the $Pmc2_1$ polymorph of $NaNbO_3$.[37] Waser et al. concluded that enhanced piezoelectric behavior was observed for submicrometer powders, in contrast to much weaker activity observed in micrometer powders. To date, there are no reports of this phase existing in powders of $NaNbO_3$ with a larger average particle size distribution.

Table 2. Structural Parameters for Sol-Gel $NaNbO_3$ from NPD Data, Using Isotropic Thermal Factors[a]

atom	site	*x*	*y*	*z*	$U(iso) \times 100$, Å^2
Nb	4c	0.2625	0.2500(5)	0.2466(5)	0.20(4)
Na	2a	0.2596(11)	0	0.7481(10)	0.50(10)
Na	2b	0.2915(12)	0.5	0.7327(11)	2.24(15)
O1	2a	0.2409(6)	0	0.3124(11)	0.53(13)
O2	2b	0.2257(5)	0.5	0.1928(11)	0.37(12)
O3	4c	0.0131(7)	0.2790(6)	0.5272(7)	1.84(9)
O4	4c	−0.0490(6)	0.2197(5)	0.0360(6)	0.61(7)

[a] Space group $P2_1ma$, $a = 5.571(1)$ Å, $b = 7.766(1)$ Å, $c = 5.513(1)$ Å, and $V = 238.52(1)$ Å^3. $\chi^2 = 4.8$, wRp = 6.6% and Rp = 6.2%.

Rietveld refinement of the model in space group $P2_1ma$ was undertaken using the model of Shuvaeva.[12] However, structural models for $NaNbO_3$ in space groups $Pn2_1a$ and $Pnm2_1$ were not available in the literature, so these were obtained by reduction in symmetry to the respective space group from *Pnma*.[38] Rietveld refinement using the space group $P2_1ma$ produced a better fit when compared with $Pn2_1a$ and $Pnm2_1$. All Rietveld refinements and specific structural parameters can be found in the Supporting Information; χ^2 values for the *Pnma*, $P2_1ma$, $Pn2_1a$, and $Pnm2_1$ Rietveld refinements are 5.8, 4.8, 5.6, and 7.9, respectively. The $Pn2_1a$ model possesses only a single Na site and can therefore be excluded. When refined in $Pnm2_1$ extremely high isotropic thermal parameters were obtained, thereby clearly indicating this not to be the correct structure. $P2_1ma$ provides the best agreement with the experimental data, and full refinement details, complete with isotropic temperature factors, can be found in Table 2. (Corresponding bond lengths obtained from refinement can be found in Supporting Information.)

At no stage in this investigation was the sol-gel sample exposed to an electric field, confirming that it is feasible to directly synthesize a noncentrosymmetric, polar phase of $NaNbO_3$; however, it is extremely difficult to produce a phase pure sample. The *Pbcm* phase of $NaNbO_3$ is consistently formed within the reaction owing, presumably, to its relative thermodynamic stability. The crystallinity of the sample was also severely reduced when compared with that produced using molten salt and solid-state techniques. The microstructure adopted displayed no regularity, with a variety of different crystal sizes and morphologies adopted throughout, as illustrated in Figure 4l, in contrast to the regularly repeating cubelike

(37) Shiratori, Y.; Magrez, A.; Kasezawa, K.; Kato, M.; Rohrig, S.; Peter, F.; Pithan, C.; Waser, R. *J. Electroceram.* **2007**, *19*, 273.
(38) *International Tables for Crystallography, Volume A, Space-Group Symmetry*, 4th ed.; Hahn, T., Ed.; Kluwer: Dordrecht, The Netherlands, 1995.

Table 3. Calculated (Using CASTEP) ^{23}Na NMR Parameters, δ_{iso}, P_Q, C_Q, and η_Q, for Selected Room Temperature Phases of $NaNbO_3$, Obtained from Both Literature and Rietveld Refinement

phase	site	δ_{iso} (ppm)	P_Q, MHz	C_Q, MHz	η_Q
		Literature			
Pbcm[7]	Na1	−4.8	2.23	2.22	0.17
	Na2	−9.0	0.96	0.87	0.79
$P2_1ma$[12]	Na1	−4.9	2.52	2.33	0.71
	Na2	−9.5	1.11	1.01	0.8
Pmma[10]	Na1	−9.4	−1.25	−1.25	0.07
	Na2	−9.4	−1.19	−1.19	0.06
		Refinement			
Pbcm	Na1	−4.8	2.27	2.27	0.07
	Na2	−8.9	0.96	0.89	0.71
$P2_1ma$	Na1	−5.7	2.47	2.22	0.85
	Na2	−9.9	−0.89	−0.80	0.82
$Pnm2_1$	Na1	−8.4	1.61	1.61	0.13
	Na2	−7.3	−2.04	−1.88	0.74
Pnma	Na1	−7.7	1.60	1.28	0.86
$Pn2_1a$	Na1	−7.7	1.43	1.25	0.98

microstructure adopted in the molten salt samples. The reduction in crystallinity is also highlighted by broadening of the ridges observed in the ^{23}Na MQMAS NMR spectrum (Figure 7c) and in all diffraction patterns collected.

Calculations. In conjunction with experiment, ^{23}Na density functional theory (DFT) calculations were completed to aid with spectral interpretation. Using the CASTEP[30] code, it was possible to predict the NMR parameters δ_{iso}, C_Q, and η_Q for any structural model and to compare them with the experimental values obtained. Initially, structures reported within the literature were calculated in order to establish the feasibility and accuracy of the calculations for $NaNbO_3$. Similar calculations were completed by Ashbrook et al.,[17] using both CASTEP and WIEN2k, and our results are in good agreement.

The NMR parameters for several $NaNbO_3$ phases suggested in the literature[39] were calculated and compared with the experimental NMR parameters. Two structures in particular, namely, *Pbcm* and $P2_1ma$, displayed good correlation with experiment after geometry optimization (allowing both the unit cell and atomic positions to vary), suggesting that the structure was perhaps not an energy minimum initially. All NMR parameters calculated for literature phases of $NaNbO_3$ (after optimization) are listed in Table 3. Parameters were also calculated using structures obtained from Rietveld refinement of our NPD data; post optimization values are also listed in Table 3. For completeness phases containing a single Na site, namely, *Pnma* and $Pn2_1a$, were also calculated which aided further in eliminating them from our investigation as plausible secondary phases. All parameters calculated for each phase prior to optimization can be found in the Supporting Information. Consistently *Pbcm* and $P2_1ma$ provided the best agreement with experiment (both from the literature and Rietveld refinement), as they appear to correlate with each of the phases identified. In particular the C_Q values obtained were in reasonable agreement, as highlighted by comparison of the solid-state NMR (9.4 T) data in Table 1 and the calculated parameters for *Pbcm* and $P2_1ma$ (Table 3). Note that the sign of C_Q, although displayed for calculated values, is not determined by experiment. The asymmetry parameter, η_Q, displayed the greatest degree of discrepancy with experiment; however, this was a consistent finding with all structures calculated. This poor agreement has been observed previously, for example, in the aluminophosphate framework AlPO-14.[40] It is noted that C_Q depends upon one principal tensor component, V_{ZZ}, whereas η_Q depends upon all three. Similar differences were also highlighted for the WIEN2k calculations completed by Ashbrook at al.[17]

Discussion

Overlaid two-dimensional ^{23}Na NMR spectra for solid-state sample A, molten salt, and sol-gel samples are shown in Figure 8. Expansions of the upper and lower sets of ridges are also shown. All four distinct Na sites present in Solid-State Sample A correlate with those present in the sol-gel sample. In particular, the two Na sites with $\delta_1 = -7.1$ and 13.5 ppm in the sol-gel sample align exactly with the second phase consistently found in all solid-state and molten salt samples, as illustrated in the overlaid isotropic projections in Figure 8b, thereby suggesting that the phase produced by sol-gel is consistently present in all samples, irrespective of synthesis route. The quantity produced, however, varies significantly depending upon synthesis method.

In a manner similar to solid-state reactions, sol-gel methods can be difficult to control. It is often challenging to accurately monitor reaction temperatures during the reflux stage of the sol-gel synthesis owing to subtle differences between internal and external vessel temperatures. In addition, during the annealing stage of the reaction it is difficult to ensure complete mixing of the reagents, which can routinely lead to impurities forming that are often challenging to remove. Within our reactions $Na_2Nb_4O_{11}$ was consistently formed.[41] There are therefore several contributing factors within the sol-gel reaction that aid in determining the exact polymorphs of $NaNbO_3$ produced.

Conclusions drawn from the ^{23}Na NMR data aided considerably in the interpretation and structural refinement of both the s-PXRD and NPD data for Solid-State Sample A. Prior to such conclusions a variety of potential orthorhombic structures similar to *Pbcm* were tested using multiphase refinements, with little success. The potential identification of the $P2_1ma$ polymorph of $NaNbO_3$ by NMR in both the solid-state and molten salt samples provided a plausible structure to test by Rietveld refinement. Therefore, multiphase refinements were completed on both the s-PXRD and NPD data obtained for solid-state sample A using the previously obtained *Pbcm* and $P2_1ma$ models and are shown in Figure 9a and Figure 9c, respectively. These models were fixed, with only lattice parameters and phase fractions being refined. Upon the addition of the $P2_1ma$ phase the quality of refinement improved considerably for both data sets. Subtle peak splittings previously treated as single phase in the synchrotron data were now accounted for and indexed which, in turn, assisted in the accurate modeling of both the profile parameters and peak intensities. Considerably better wRp (14.2%) and χ^2 (7.6) values were obtained, with refined phase fractions of 60(2)% and 40(2)% for the *Pbcm* and $P2_1ma$ phases, respectively. A similar two-phase refinement of the neutron data considerably improved the quality of the fit at low *d*-spacing, in comparison to the single phase refinements previously discussed, leading to better wRp (8.4%) and χ^2 (22.7) values, with refined phase fractions of 57(2)% and 43(2)% for the *Pbcm* and $P2_1ma$ phases, respectively. The phase fractions obtained from refinement are in agreement with those from NMR (estimated to be ∼60% and ∼40%) from the MQMAS spectrum in Figure 5b. In particular, the additional peaks previously

(39) I *norganic Crystal Structure Database*; Fachinformationszentrum (FIZ): Karlsruhe, Germany, 2007.

(40) Ashbrook, S. E.; Cutajar, M.; Pickard, C. J.; Walton, R. I.; Wimperis, S. *Phys. Chem. Chem. Phys.* **2008**, *10*, 5754.

(41) Jahnberg, L. *J. Solid State Chem.* **1970**, *1*, 454.

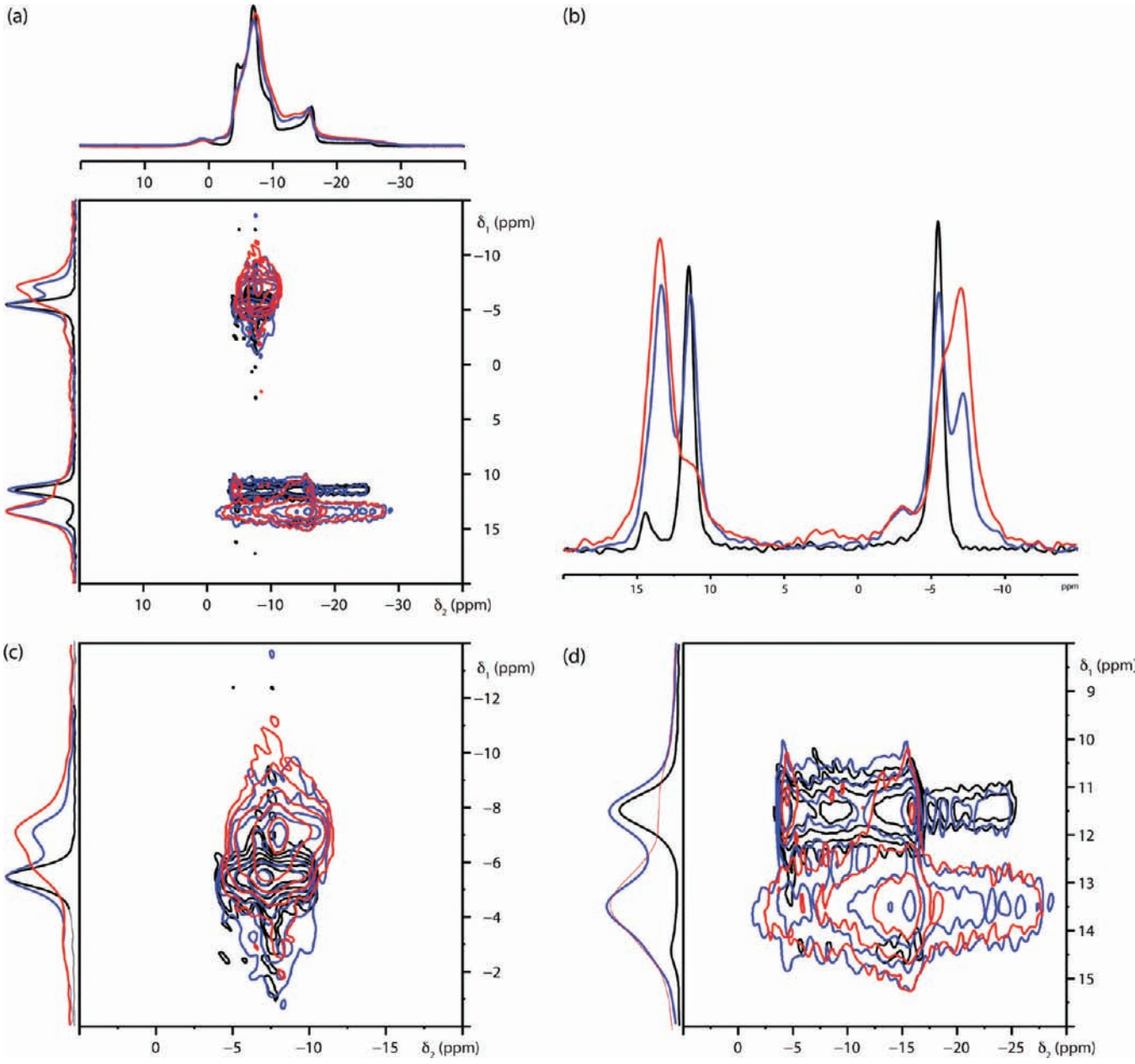

Figure 8. ^{23}Na (9.4 T) NMR of phase pure *Pbcm* $NaNbO_3$ (shown in black and synthesized using molten salt methods, 1000 °C for 24 h), Solid-State Sample A $NaNbO_3$ (shown in blue), and sol-gel $NaNbO_3$ (shown in red): (a) conventional MAS and triple-quantum MAS NMR spectra; (b) corresponding isotropic projections; (c, d) expansions showing the upper ($\delta_{iso} = -5.08$ ppm and $\delta_{iso} = -4.24$ ppm) and lower ($\delta_{iso} = -0.51$ ppm and $\delta_{iso} = 1.44$ ppm) ridges.

highlighted in the single phase refinement at 2.47 and 2.49 Å were now adequately accounted for, as shown in Figure 9d. However, on closer inspection of the refinements involving the suggested $P2_1ma$ phase, it is apparent that subtle peak broadenings exist that are compatible with a symmetry-lowering to monoclinic ($\beta \neq 90°$). Such a symmetry-lowering has previously been observed in the KNN solid-solution at low potassium content.[42] The highly subtle nature of this in the present case precludes a complete analysis, but further details are provided in the Supporting Information. We shall now refer to this phase as "$P2_1ma$", on the understanding that it appears very subtly monoclinic. Refined lattice parameters for multiphase refinement of Solid-State Sample A using both NPD and XRD data are provided in Supporting Information.

The space group $P2_1ma$ was a tentative suggestion by Ashbrook et al.[17] for the nature of the unknown phase within their sample, made purely by a preliminary examination of the additional peaks in their l-PXRD pattern. Despite their sample being reasonably crystalline (synthesized using hydrothermal methods), it would have been considerably challenging to unambiguously distinguish such peaks. Although high-resolution data are usually required to draw such conclusions, in this particular case their tentative suggestion appears to have been borne out. Their explanation of why the "$P2_1ma$" polymorph is formed perhaps relates to their use of a low temperature synthetic route (200 °C) as opposed to conventional solid-state methods using temperatures in excess of 1000 °C. We have

(42) Zhang, N.; Glazer, A. M.; Baker, D. W.; Thomas, P. A. *Acta Crystallogr.* **2009**, *B65*, 291.

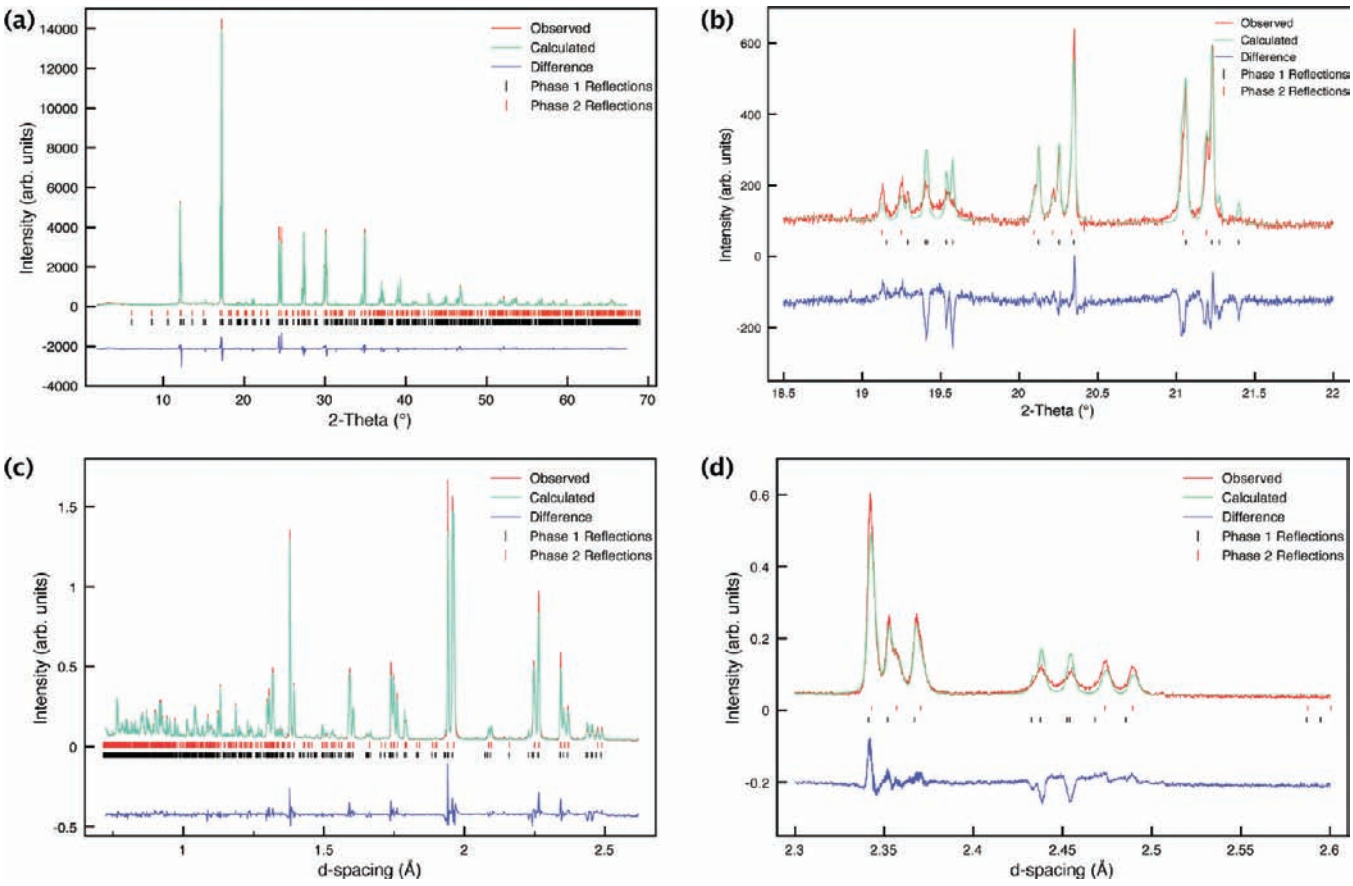

Figure 9. Multiphase Rietveld profiles for Solid-State Sample A $NaNbO_3$ using structural models *Pbcm* and $P2_1ma$ for (a, b) s-PXRD data and (c, d) NPD data. Expansions of the corresponding superstructure peaks are shown in (b) ($2\theta = 18.5-22°$) and (d) (2.3−2.6 Å).

shown, using a variety of techniques, that this "$P2_1ma$" polymorph is consistently formed, regardless of specific experimental conditions. Their suggestion of why is also consistent with our findings; temperature plays a prominent role in the phases of $NaNbO_3$ synthesized and their relative quantities.

The two polymorphic phases of $NaNbO_3$, *Pbcm* and "$P2_1ma$", routinely coexist in many samples irrespective of synthesis route and are seen, from both diffraction and solid-state NMR, to be structurally similar. However, crystallographic examination shows that the two adopt subtly different octahedral tilt systems. This cooperates with local Na^+ cation displacements to produce both a centrosymmetric and a polar phase of similar stability. In the *Pbcm* phase the Na displacements are out-of-phase with one another, leading to the longer periodicity of the *c*-axis ($4a_p$ or about 15.5 Å), as shown in Figure 1a. The mechanism of octahedral tilting within the *Pbcm* structure is effectively a "twinning" operation when compared with $P2_1ma$ (or more strictly the parent *Pnma*). Hence the standard $a^-a^-b^+$ system in $P2_1ma$ becomes $[a^-a^-b^+/a^-a^-b^-/a^-a^-b^+]$ via an inversion about the central block (equivalent to an additional out-of-phase tilt between blocks 2 and 3 along the *c*-axis). It is perhaps therefore of little surprise that two polymorphs based on these very similar tilt systems can compete, depending on synthetic variables, and also no surprise that their diffraction patterns are so similar. In fact, a further manifestation of the similarity of the two structures can be seen in the NPD data (Figure 9d), where the additional superlattice peaks due to the $4a_p$ supercell in the *Pbcm* phase (i.e., the l-odd reflections) are noticeably broader than the subcell peaks, suggesting that long-range registry of the additional out-of-phase tilt is weak.

The subtle effects that drive the appearance of both polymorphs are currently unknown, but the influence of the "ferroelectrically active" Nb^{5+} cation on the B-site must be considered. In the case of $NaNbO_3$, diffraction indicates that in the *Pbcm* phase Nb "on average" lies approximately centrosymmetrically within the octahedra. However, the local environment probe, solid-state NMR, suggests it may be disordered in some manner. The ^{93}Nb MQMAS NMR spectrum recorded for the commercially purchased sample (Figure 2c) displays a degree of additional broadening, suggesting that Nb may exhibit some positional disorder. In the "$P2_1ma$" polymorph the Nb^{5+} cation lies significantly off-center in a polar manner (toward an edge of the octahedron).

Ultimately, the use of several complementary techniques within this investigation has led to the accurate structural identification of two polymorphic room temperature phases of $NaNbO_3$ present in a variety of samples synthesized by various synthetic routes. Previous studies have often concentrated solely on one particular characterization technique. However, as presented within this particular study, it can be extremely challenging, and dangerous, to rely on such an approach. Using diffraction alone for example, it can be difficult to identify and correctly model weak superlattice peaks and peak splittings or broadenings. In such cases it is vital to utilize a number of different techniques in order to ensure an accurate and robust structural characterization.

Conclusions

In summary we have confirmed it is possible to synthesize a polar phase (probably monoclinic but of symmetry very close

to orthorhombic, space group $P2_1ma$) of $NaNbO_3$ using sol-gel techniques. We have also shown, by means of a systematic study, that synthetic method affects the polymorphic forms of $NaNbO_3$ produced in any one reaction. It is possible to isolate a pure sample of the *Pbcm* polymorph, and high-resolution powder diffraction studies confirm that this is indeed a correct space group assignment for this phase; previous confusion regarding the possibility of a symmetry-lowering to monoclinic might be explained by the occurrence of a significant "$P2_1ma$" phase impurity in the sample studied by Darlington and Knight (refer to Supporting Information).[5] Routinely the phases *Pbcm* and "$P2_1ma$" coexist as the two major room temperature polymorphs of $NaNbO_3$. The thermodynamic stabilities of the two phases are believed to be extremely similar; therefore, slight variations in the reaction conditions forces one to preferentially form over the other. Consistently, the *Pbcm* polymorph forms more readily, suggesting it to be the more thermodynamically stable of the two. Finally, we emphasize that it is essential to be aware of this subtle polymorphism in $NaNbO_3$, its occurrence as a function of preparative method, and how to identify it from both diffraction and NMR data; much of the earlier work regarding $NaNbO_3$ and its phase diagram should be treated with some degree of caution in light of our findings. Furthermore, these findings have implications for the present and future study of the KNN solid-solution and its piezoelectric behavior.

Acknowledgment. We thank undergraduate students Pierre-Yves Calvez and Charlotte H. L. Cree for their contributions to this work. This work was carried out with the support of the Diamond Light Source. We thank Dr. Manfred Buck for his assistance with the SHG measurements and Dr. John Griffin, Dr. Thushitha Mahenthirarajah, Sandra Reisinger, and Alexandra Gibbs for experimental assistance. All DFT calculations were completed using the EaStCHEM Research Computing Facility, which is partially supported by the eDIKT initiative. We also acknowledge the EPSRC for support (Grant EP/E041825/1) and the award of a studentship to Karen E. Johnston.

Supporting Information Available: Additional Rietveld refinements, complete two-dimensional ^{23}Na MAS NMR spectra, and SHG measurements. This material is available free of charge via the Internet at http://pubs.acs.org.

JA101860R